Behaviour of square hollow structural steel braces with end connections under reversed cyclic axial loading

Brad Shaback and Tom Brown

Abstract: The hysteretic behaviour of nine square hollow structural steel (HSS) sections with gusset plate end connections subject to inelastic cyclic loading has been examined by an experimental investigation. Brace slenderness ratio, width to thickness ratio, and to a lesser extent, the end connection were identified as the key parameters in the tests. It was shown that the effective slenderness ratio is the most important parameter governing the hysteretic behaviour. The out-of-plane deflection of the brace can be accurately calculated using a simplified geometrical model or a model calibrated against the test results. Reduced compressive capacity as specified by the current Canadian Standards Association (CSA) standard was nonconservative for the specific loading sequence employed in this series of tests. Quantification of the energy dissipation proved that the gusset plates account for a small percentage of the total energy dissipated. The experimental fracture life of the specimens proved to be most affected by the width to thickness ratio and the effective slenderness ratio. An empirical equation is proposed to more accurately determine the theoretical fracture life of an HSS brace.

Key words: brace, hysteresis, steel, hollow structural section, cyclic, end connection, fracture, energy dissipation, compressive capacity, effective slenderness ratio.

Résumé : Le comportement hystérétique de neufs profilés carrés tubulaires (« hollow structured steel : HSS ») en acier munis de goussets aux extrémités et sujets à un chargement cyclique inélastique a été examiné lors d'essais. Le rapport d'élancement des contreventements, le rapport largeur à épaisseur et, d'une façon moindre, l'articulation d'extrémité ont été identifiés comme étant les paramètres clés dans les tests. Il est démontré que le rapport d'élancement effectif (« effective slenderness ratio ») est le paramètre le plus important sur le comportement hystérétique. Le fléchissement déporté (« out-of-plane deflection ») du contreventement peut être calculé avec précision en utilisant un modèle géométrique simplifié ou un modèle étalonné avec les résultats des tests. La capacité réduite en compression, telle que spécifiée par la norme de l'Association canadienne de normalisation (CSA) en vigueur, est non conservatrice pour la séquence de charge spécifique employée dans cette série de tests. La quantification de la dissipation d'énergie prouve que les goussets comptent pour un faible pourcentage de l'énergie totale dissipée. L'endurance expérimentale à la rupture (« experimental fracture life ») des spécimens est plus affectée par le rapport largeur à épaisseur et le rapport d'élancement effectif. Une équation empirique est proposée afin de déterminer plus précisément l'endurance théorique à la rupture d'un contreventement HSS.

Mots clés : contreventement, hystérèse, acier, profilé tubulaire, cyclique, articulation d'extrémité, rupture, dissipation d'énergie, capacité en compression, rapport d'élancement effectif.

[Traduit par la Rédaction]

Introduction

Energy dissipation during the seismic response of steel structures derives from various sources, including the nonlinear behaviour of structural elements. The concentrically braced steel frame (CBF) dissipates energy primarily through yielding and buckling of the brace members. It is a commonly used lateral load resisting system and has many advantages over other systems. The CBF is easy to design, detail, and construct, and energy is dissipated efficiently through axial forces in the braces. The system is stiff, minimizing drift, in turn minimizing damage to nonstructural components. Disadvantages of the CBF include low redundancy, degradation in brace compressive capacity, and the potential for low cycle fatigue failure.

Previous research has determined that the principal characteristics of braces affecting hysteresis are effective slenderness ratio, end conditions, and section shape (Bruneau et al. 1998). Earlier test programs have focused on these aspects through testing of members of limited sizes. This series of tests will increase the amount of useful data

Received 5 September 2001. Revision accepted 19 March 2003. Published on the NRC Research Press Web site at http://cjce.nrc.ca on 11 August 2003.

B. Shaback[1,2] and T. Brown. Department of Civil Engineering, University of Calgary, 2500 University Drive NW, Calgary, AB T2N 1N4, Canada.

Written discussion of this article is welcomed and will be received by the Editor until 31 December 2003.

[1]Corresponding author (e-mail: bshaback@ademengineering.com).
[2]Present address: ADEM Engineering Consultants, Suite 222, 222-58th Avenue SW, Calgary, AB T2H 2S3, Canada.

 doi: 10.1139/L03-028

necessary for modeling bracing members by testing section sizes closer to those used in practice. Effective slenderness ratios were varied but were less than the maximum specified by CAN/CSA-S16-01 (CSA 2001). End conditions comprised rectangular gusset plate connections with variable flexural strength and stiffnesses. Only square hollow structural steel (HSS) sections were used in these tests. Popov and Black (1981) found HSS braces to exhibit superior performance as a result of their higher radii of gyration and resistance to local buckling for the same cross-sectional area, relative to other rolled shapes.

Because brace behaviour is difficult to predict analytically, it is important to gather data from experiments on brace behaviour. Quantification of the brace behaviour is integral to the development of new analytical models, as well as calibration of existing models, for the design of braced frames. Hysteretic behaviour (axial load – axial displacement), out-of-plane deflection, compressive capacity degradation, energy dissipation, and low cycle fatigue failure characteristics are examined using the results of these tests.

Experimental program

Test specimens

The purpose of the experimental program was to investigate the behaviour of full-scale HSS braces with typical end connections under cyclic axial loading. Nine specimens from various sized square HSS were tested until failure. Hot-rolled rectangular gusset plates provided end connections. Specimens were fabricated from CSA G40.21-M 350W Class C square HSS and 300W structural-quality steel for the gusset plates. Complete information on the specimen configuration and details of specimens are given in Fig. 1 and Tables 1 and 2. The effective length factor, K, was determined accounting for the stiffness of the gusset, using the method of Jain et al. (1978).

All specimens were designed to conform to the requirements of CAN/CSA-S16-01 Clause 27.4 (CSA 2001) for the design of diagonal bracing members and bracing connections for ductile, concentrically braced frames. Central to the requirements of this clause are the following equations, limiting the slenderness ratio (L/r, where L is the overall specimen length and r is the radius of gyration) and the width to thickness ratio (b/t) of a brace to maximize the energy dissipation and delay or prevent the onset of local buckling in the bracing member:

$$[1] \qquad \frac{L}{r} \le \frac{1900}{\sqrt{F_y}} \le 101.6 \qquad \text{if } F_y = 350 \text{ MPa}$$

$$[2] \qquad \frac{b}{t} \le \frac{330}{\sqrt{F_y}} \le 17.6 \qquad \text{if } F_y = 350 \text{ MPa}$$

Specimen slenderness ratios varied from 69 to 93. Similarly, all HSS specimen width to thickness ratios fell within the limits of the CSA standard (Table 2). Gusset plates were designed such that their axial strength was greater than that of the HSS and were detailed to avoid brittle failure due to the rotation of the brace when it buckles. A gusset plate free length ranging from 1.25 to 2.00 times the thickness of the gusset plate was used. This free length, suggested by previous research (Astaneh-Asl et al. 1985) to be twice the thickness of the gusset, is to allow for the free formation of a plastic hinge when the gusset plate is connected to the adjacent framing members along a single free edge.

The test specimens were fabricated by cutting a longitudinal slot in the flanges of the HSS specimen and welding the gusset plate into this slot. Weld lengths between the gusset plate and the HSS specimen were proportioned based on the work of Korol (1996). Korol found that the shear lag requirements of CAN/CSA-S16.1-94 (CSA 1994) did not explicitly cover HSS tension members with welded and slotted connections. Therefore, HSS sections were treated similarly to open shaped sections, resulting in overly conservative requirements. Using suggestions of Korol, the specimen weld lengths were greatly reduced from those dictated by the requirements of CAN/CSA-S16-01 (CSA 2001). Further, welds were returned across the thickness of the gusset plate. This, according to Cheng et al. (1998), permits the assumption that the full cross section of the tube is available to carry the load when the effects of shear lag are calculated.

Test setup and instrumentation

The test frame assembly is shown schematically in Fig. 2. Two 1.5 MN hydraulic actuators were coupled to provide up to 3.0 MN of load through a distribution beam. Load is resisted in the frame by similar beams composed of channel pairs at the back end of the actuators and at the opposite end of the specimen. Two W360 × 179 steel sections link the front and back of the test frame assembly. These wide flange members complete a closed-loop system. The specimen gusset plates were welded to 76.2 or 88.9 mm thick plates using full-penetration welds. These were then bolted, using short lengths of DYWIDAG prestressing bars, to similar plates that were part of the load frame.

Strain gauges were placed in pairs at various locations at the midspan of the HSS and at approximately 7% of the specimen length on either side of the midspan. String potentiometers were used to measure the axial and out-of-plane displacements of the specimen. The cyclic axial load applied to the specimens was measured using the 1.5 MN load cells located between the actuators and the distribution beam. The summation of the loads measured by each actuator provided the total axial load on the specimen.

Test procedure

The test specimens were subject to quasi-statically applied cycles of reversing axial displacement. To maintain some continuity in the results, all specimens were initially subject to compressive loads followed by tensile loading. Displacement rates varied for each cycle; however, the average cycle times were nearly equal. Test specimens were initially subject to three elastic cycles, two at approximately 25% of the nominal yield load and the third at approximately 75%. The elastic cycles allowed for an instrumentation calibration check and provided a good opportunity to ensure the test frame assembly was operating safely. A typical loading sequence for each specimen is shown in Fig. 3. All specimens were subject to similar loading sequences. After the initial elastic cycles, the specimens were loaded into their inelastic region to a prescribed level of axial displacement predetermined as a specified level of ductility. The displacements were continuously increased until the specimen failed as a

Fig. 1. Specimen configuration: (*a*) elevation; (*b*) plan view.

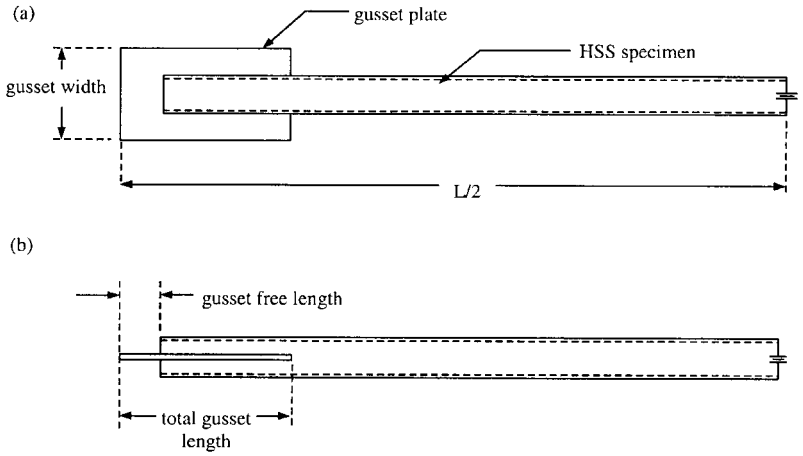

Table 1. Details of specimens tested.

Specimen	HSS designation ($b\times d\times t$)	Total specimen length, L (mm)	K	KL/r	Gusset dimensions (mm) Free length	Total length	Width	Thickness	E (GPa)	F_y (MPa)[a]
1A	127×127×6.4	3450	0.74	52.3	50	350	200	25.4	196	461
1B	127×127×8.0	3452	0.75	53.9	51	351	225	25.4	191	421
2A	152×152×8.0	4040	0.77	53.3	45	395	250	25.4	202	442
2B	152×152×9.5	4028	0.75	52.4	39	389	300	25.4	196	442
3A	127×127×6.4	4456	0.71	64.8	53	353	200	25.4	196	461
3B	127×127×8.0	4446	0.71	65.8	48	348	225	25.4	191	421
3C	127×127×9.5	4414	0.66	61.6	32	332	250	25.4	202	461
4A	152×152×8.0	4944	0.75	63.5	47	397	250	25.4	202	442
4B	152×152×9.5	4914	0.70	59.7	32	382	300	25.4	196	442

[a]Offset of 0.2%.

Table 2. Specimen dimensions.

Specimen	HSS designation ($b\times d\times t$)	Thickness (mm)	Width (mm)	Depth (mm)	Flat width (mm)	Flat depth (mm)	b/t	$330/(F_y)^{1/2}$	Area (mm^2)
1A	127×127×6.4	6.36	127.9	126.7	96.2	97.03	15.10	15.4	3070
1B	127×127×8.0	na	na	na	na	na	na	16.1	na
2A	152×152×8.0	8.01	154.2	151.2	115.5	118.10	14.40	15.7	4645
2B	152×152×9.5	9.24	152.8	151.2	111.8	114.30	12.10	15.7	5308
3A	127×127×6.4	6.46	127.4	126.4	96.7	97.20	15.00	15.4	3114
3B	127×127×8.0	7.65	128.0	126.1	92.5	92.80	12.10	16.1	3665
3C	127×127×9.5	9.42	127.2	126.1	84.2	82.40	8.93	15.4	4423
4A	152×152×8.0	8.09	153.5	151.6	117.9	117.50	14.60	15.7	4695
4B	152×152×9.5	9.18	152.4	150.7	109.6	112.50	11.90	15.7	5246

Note: na, not available.

result of fracturing at the central hinge, always in a tension cycle. Figure 4 illustrates a specimen during a test.

Ancillary tests

Five separate HSS sizes were used in this series of tests. Three stub-column test sections were removed from the same material used to fabricate the test specimens. The stub-column testing procedure was employed. This procedure is outlined by the Structural Stability Research Council (SSRC) (Galambos 1998) and involves a static compression test on the full cross section of the HSS. Stub-columns were cold-sawn from the parent material to lengths specified by the SSRC requirements. The yield stress and strain for the stub-columns were obtained using the 0.2% offset method. A summary of the material properties for each specimen is provided in Table 1.

Brace test results

Out-of-plane deflection

A large proportion of repair costs to structures sustaining damage during seismic events is related to the damage of nonstructural components. This can be because of such ef-

Fig. 2. Test frame assembly.

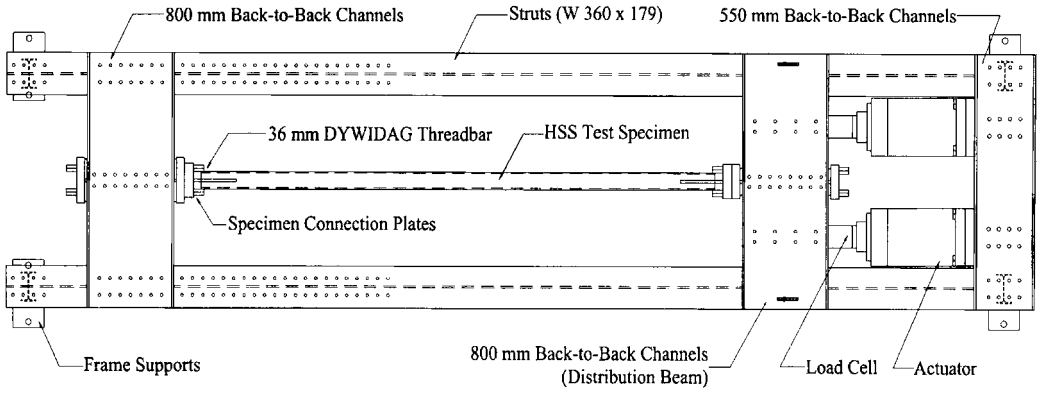

Fig. 3. Typical loading sequence.

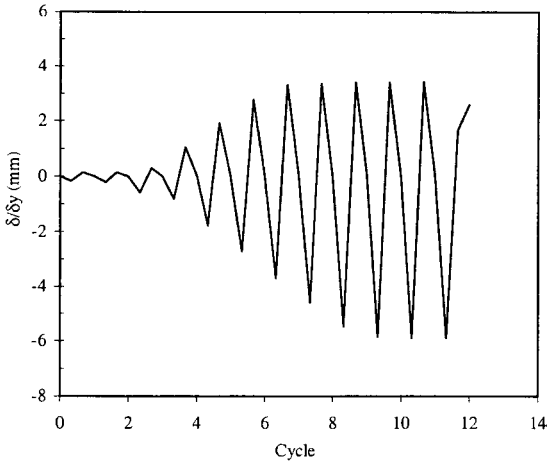

fects as high lateral frame drift or, in the case of a braced frame, out-of-plane deflection of the brace. This type of damage was evident in many braced frames in the 1995 Hyogo-ken Nanbu earthquake (Tremblay et al. 1996), where a buckling brace shed surrounding wall finish. With knowledge of the extent to which a brace may deflect out-of-plane, damage can be avoided in the nonstructural components adjacent to a buckling brace.

Two approaches are presented to predict the out-of-plane deflection (Δ) of a simple brace: a general, simplified equation based on the geometry of a buckled brace and an equation developed from and calibrated against the data from this series of tests.

Results show that the out-of-plane deflection was strongly dependant on the plastic rotation at the gusset plate and central specimen hinges. This relationship was also observed by Archambault (1995). Other parameters such as effective slenderness ratio and width-to-thickness ratio had considerably less influence on the out-of-plane deflection.

The simple, geometrical approach is presented in eq. [3]:

$$[3] \qquad \Delta = \sqrt{\frac{\delta}{2}\left(L - \frac{\delta}{2}\right)}$$

where δ and L represent the axial deflection and specimen length, respectively. Equation [3] overestimates the out-of-plane deflection at low ductility levels and underestimates it at higher levels. This is to be expected because the specimen behaves as a mechanism with plastic hinges at the end connections and at midspan when subject to higher ductilities. At lower levels of ductility, however, the specimen remains elastic and does not exhibit the same deflected shape. Therefore, to develop an equation for the out-of-plane deflection of a brace applicable at all ductility levels, it is necessary to calibrate it with respect to actual data. Equation [4], derived from the data, gives the lateral displacement, normalized with respect to specimen length, as a function of the ductility, μ:

$$[4] \qquad \frac{\Delta}{L} = -\frac{1}{9}(\mu)^{1.9} + 2\mu$$

Equation [4] provides excellent correlation of the out-of-plane deflections of a brace, at all ductility levels. The results from this series of tests are compared in Fig. 5 with the curves predicting out-of-plane deflection developed from eqs. [3] and [4].

Compressive resistance

The compressive resistance values of the specimens tested are compared with the nominal (unfactored) resistance values suggested by CAN/CSA-S16-01 (CSA 2001) and AISC (1999). Compressive resistances in cycles following the initial buckling cycle were also examined.

Comparison of the experimental initial compressive resistance with the CSA standard specified unfactored resistance showed very good results, with a mean experimental to theoretical ratio of 1.01 and a coefficient of variation of 0.095. Although the AISC standard values tend to be less conservative, the results were very similar. One exception in the results was that of specimen 3C. This specimen had an initial compressive capacity in the order of 82% of that which the CSA standard suggests. There was a possibility that additional eccentricity was introduced into the specimen during the welding of the gusset plates to the thick end connection plates used to fix the specimen to the testing frame.

The compressive peak loads of the braces in load cycles following the initial buckling cycle show a marked decrease, approximately 25% in the second inelastic cycle, and thereafter increasing, for all specimens. This is a typical response of braces subject to inelastic cyclic loading and can be attributed to two effects: residual lateral displacement at the start of a compressive cycle and Bauschinger effects. Bauschinger effects are characterized by a decrease in the

Fig. 4. Example of test.

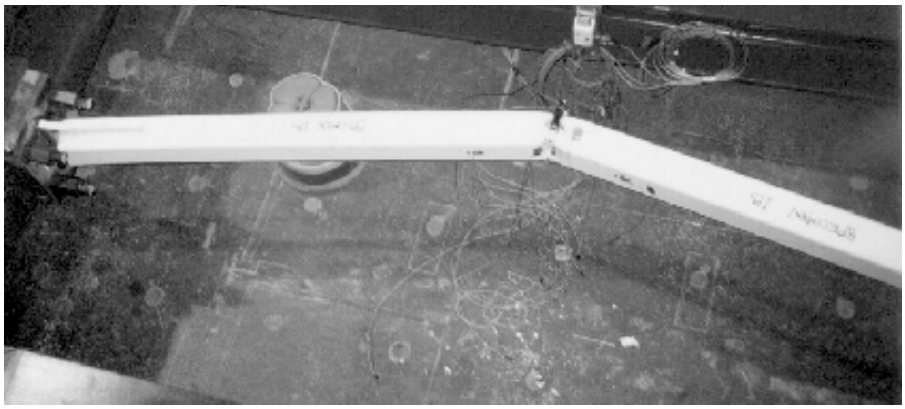

Fig. 5. Comparison of out-of-plane deflection equations.

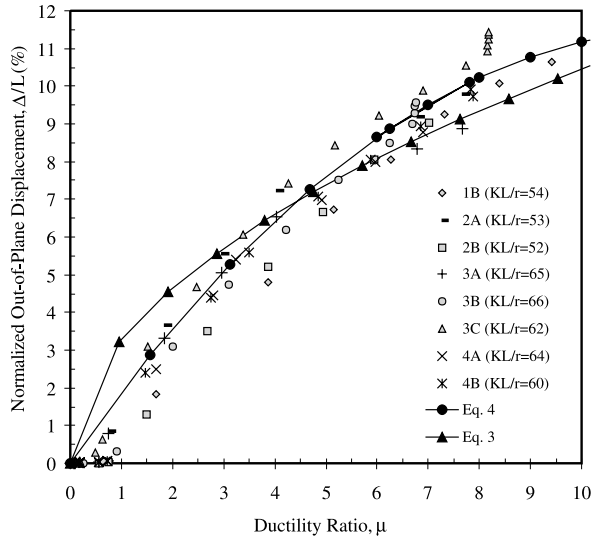

proportional limit and yield strength by straining a plastically deformed specimen in the opposite sense.

The current CSA standard requires that the degradation in compressive resistance be accounted for when designing a ductile braced frame. The standard suggests the following equation for the reduced compressive resistance, C_r':

$$[5] \qquad C_r' = C_r\left(\frac{1}{1+0.35\lambda}\right)$$

where the initial unfactored buckling capacity, C_r, is given as

$$[6] \qquad C_r = AF_y(1+\lambda^{2n})^{-1/n}$$

where A is the cross-sectional area of the HSS, n is a parameter for compressive resistance, and

$$[7] \qquad \lambda = \frac{KL}{r}\sqrt{\frac{F_y}{\pi^2 E}} \text{ and } n = 1.34$$

where E is Young's modulus of elasticity. Equations [5] and [6] were compared with the results of the maximum compressive resistances achieved in each cycle for each specimen. This comparison is shown in Fig. 6 for specimen 1B. This result is typical for all specimens where the comparison between the nominal standard specified resistance and the measured resistance is good for the first and second buckling cycles. The maximum compressive axial load for any cycle ($P_{comp\ max}$) has been normalized with respect to the compressive resistance, C_r. It is evident from Fig. 6 that the current requirements for the degradation in compressive resistance of a brace do not adequately represent the behaviour of the specimens tested in this series. For the first cycle after the initial buckling load, the measured resistance of the specimen compares well with the suggested reduced resistance. In subsequent cycles, however, in which the standard does not specify any further reduction, the specimens continue to show a significant decrease in compressive capacity. In previous experimental programs, however, the majority of the brace capacity degradation occurs after the first buckling cycle and thereafter remains nearly constant (Kahn and Hanson 1976; Jain et al. 1978). It is believed that the discrepancy exists because of a reduction in the tensile displacement in later cycles. Owing to column growth, or residual axial elongation, the actuator stroke available for the application of subsequent tensile loads decreased with each cycle. This resulted in incomplete reduction of the residual lateral displacement for a tension cycle and, consequently, an increase in the initial lateral displacement, or eccentricity, for the next compressive cycle. In turn, the maximum compressive loads are reduced for these cycles. To achieve reduced compressive capacities in line with those suggested by the CSA standard, it would be necessary to reduce the lateral deflection to a minimum at the end of each tension cycle.

Care should therefore be exercised in assuming a lower bound for the compressive resistance of a buckled brace. Effects such as a residual lateral displacement can significantly affect this assumed capacity. In turn, this is very dependant upon the loading history seen by the brace. This conclusion was also reached by Archambault (1995) after an examination of two different loading sequences applied to similar specimens. The conclusions were very similar, with the current code equation being unable to accurately predict the reduced capacity of a brace for the particular loading sequence used.

Fracture life – low-cycle fatigue failure

The early fracture of HSS braces due to low-cycle fatigue is identified as one the disadvantages of their use in braced frame structures. Early fracture of the brace can significantly

Fig. 6. Compressive resistance degradation.

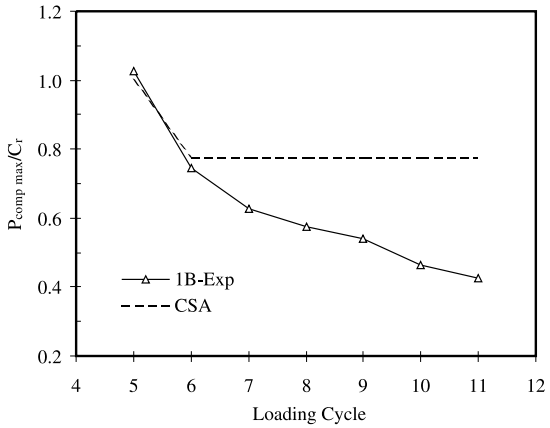

Fig. 7. Determining Δ_f.

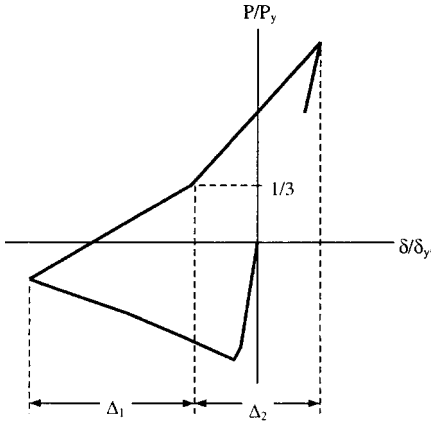

affect the lateral stiffness and the energy dissipation capacity of the braced frame.

The resistance of a brace to early fracture can be attributed to several factors. The most important of the factors affecting brace fracture life are the width to thickness ratio of the brace wall, the effective slenderness ratio, the width to depth ratio, and the mechanical properties of the brace (Tang and Goel 1987). The width to thickness ratio of the member is especially influential on the fracture life. As observed in this series of tests, the fracture of the brace followed closely after the local buckling of the compression flange in the plastic hinge region. The subsequent large, cyclic strains in this hinge region ultimately resulted in the failure of the cross section. According to elasticity theories, resistance to local buckling increases as the width to thickness ratio decreases, the local buckling strength of a plate being inversely proportional to the square of the width to thickness ratio. The column slenderness ratio has also been found to affect the fracture life of a brace (Tang and Goel 1987), with the more slender specimens experiencing less severe buckling.

Various empirical equations to predict the fracture life of bracing members have been developed, including those of Tang and Goel (1987), Hassan and Goel (1991), and Archambault (1995). Archambault's equation provides a prediction of fracture life (Δ_f) based on the geometry and mechanical properties of the specimen. This fracture life is a prediction of the cumulative deformation that a brace can withstand prior to cross-sectional failure. The experimentally determined fracture life of a tubular bracing member, $\Delta_{f\ exp}$, is a function of the cumulative deformation experienced by a specimen. This value is determined from the test results by first normalizing the hysteretic curve. A typical normalized hysteretic curve (Lee and Goel 1987) is shown in Fig. 7 with the parameters necessary for determining $\Delta_{f\ exp}$:

$$[8] \qquad \Delta_{f\ exp} = \sum (0.1\Delta_1 + \Delta_2)$$

It is evident from eq. [8] that the compressive deformation excursion is heavily discounted and the tensile deformation excursion is regarded as being the most important component of the deformation affecting the fracture life of a brace. The equation is based on the hypothesis that the tension forces applied to a straightened brace have significantly more effect on the fracture life than do tension forces applied while straightening the brace. This is reflected in the inclusion of only 10% of the compressive component of normalized axial deformation. Equation [8] is applied regardless of the relative magnitudes of the tensile or compressive excursions and therefore could be applied to any set of cyclic displacements.

The equations used to predict the fracture life of an HSS brace have been calibrated with respect to experimental data and have been subsequently refined with the addition of new data sets. The data from this series of experiments and those from the simple brace tests of Archambault (1995) have been combined to develop a more statistically reliable equation used to predict the theoretical fracture life of a brace. All of the relationships with effective slenderness ratio, width to thickness ratio, breadth to depth ratio, and yield strength are retained, with minor modifications resulting in better correlation with the data:

$$[9a] \qquad \Delta_f = C_s \frac{(350/F_y)^{-3.5}}{[(b-2t)/t]^{1.2}} \left(\frac{4(b/d) - 0.5}{5} \right)^{0.55} (70)^2 \qquad \text{for } \frac{KL}{r} < 70$$

$$[9b] \qquad \Delta_f = C_s \frac{(350/F_y)^{-3.5}}{[(b-2t)/t]^{1.2}} \left(\frac{4(b/d) - 0.5}{5} \right)^{0.55} \left(\frac{KL}{r} \right)^2 \qquad \text{for } \frac{KL}{r} \geq 70$$

where C_s is an experimentally determined constant equal to 0.065. Equations [9*a*] and [9*b*] give the normalized (nondimensional) fracture life in terms of the principal variables (F_y in megapascals). The comparison between the experimental fracture life (eq. [8]) and the prediction of fracture life using eqs. [9*a*] and [9*b*] is shown in Fig. 8. The result is an improved prediction of fracture life. Statistically, the equation has a mean of 1.00 and a standard deviation of 0.36. This represents a 50% reduction in the standard deviation over previous, similar, fracture-life equations. This equation can be incorporated into models that use HSS members as braces subject to inelastic loading cycles and local buckling.

Fig. 8. Fracture life.

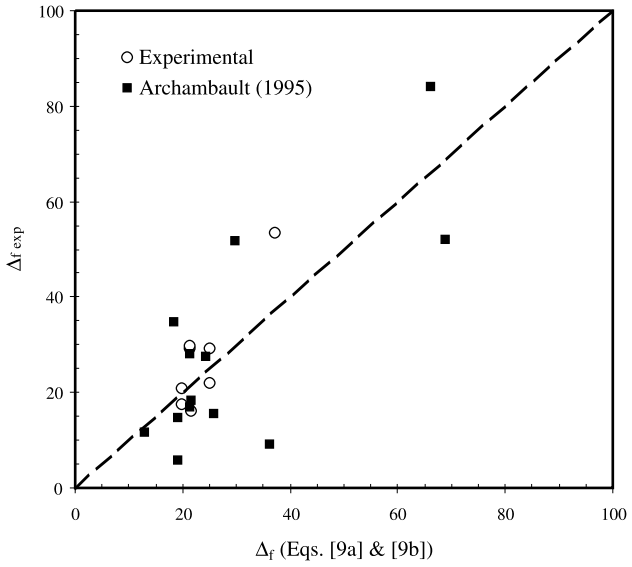

Fig. 9. Hysteretic curve.

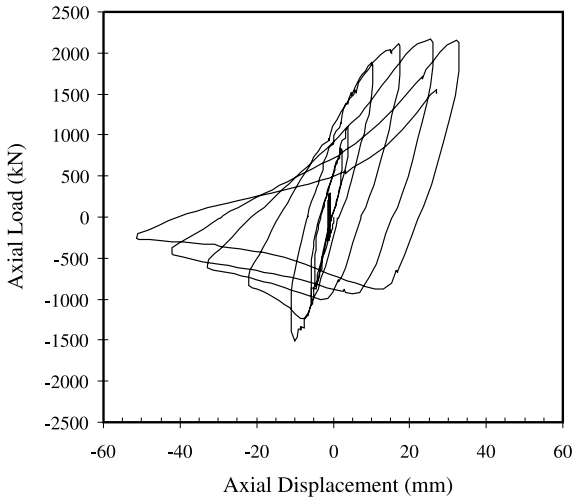

Fig. 10. Normalized hysteretic curve comparison.

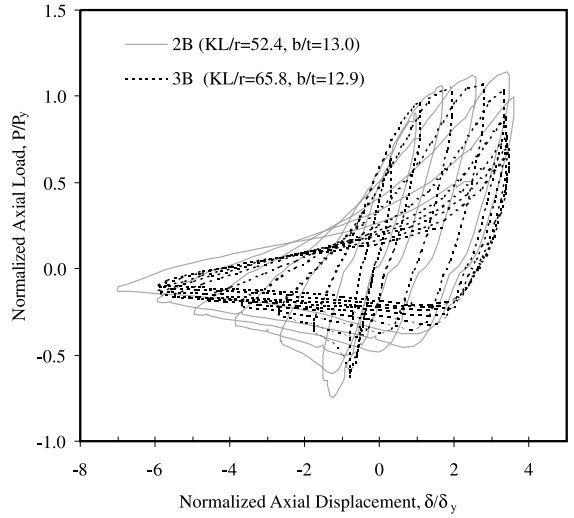

Hysteretic behaviour and energy dissipation

A hysteretic curve for specimen 2A is presented in Fig. 9. The general shape of the hysteretic loops displayed by each specimen was typical of an intermediate length brace member subject to inelastic cyclic loading. The degradation in compressive capacity after the initial buckling cycle was evident in the hysteretic behaviour of all specimens. Other important phenomena observed from the hysteretic loops included a loss of axial compression stiffness, residual axial displacement, and a loss of tangent stiffness at zero applied load.

The normalized hysteretic loops of specimens 2B and 3B are compared in Fig. 10. The normalization of a hysteretic loop is useful to compare the hysteretic behaviour of different specimens. These specimens have essentially the same width to thickness ratio but different effective slenderness ratios. Specimen 2B (KL/r = 52.4), which is stockier than specimen 3B (KL/r = 65.8), exhibits better hysteretic behaviour in compression in the form of a fuller loop. The specimens have nearly identical behaviour in tension, with the exception of the small difference in loop area upon reloading of the specimen in tension. The specimen with the smaller effective slenderness ratio is stiffer in this region and therefore is capable of dissipating more energy. As the effective slenderness ratio decreases, the stiffness degradation decreases. Specimen 2B also displays slightly better behaviour at maximum tensile loads.

The width to thickness ratio, b/t, has a minor influence on the hysteretic loops of the specimens. As b/t decreases, the specimen is capable of sustaining more loading cycles, which, for the current test program, results in greater maximum displacements in the later cycles.

The energy dissipated by each specimen was quantified. The area enclosed by the axial load – axial displacement curves represents the hysteretic energy dissipated by the test specimens. The majority of the dissipated energy is a result of the tension yielding and inelastic buckling of the HSS. A lesser part of the total energy dissipated is a result of the stable plastic rotation of the end connections that continues after the HSS buckles.

The total cumulative energy dissipated by the system, both end connections and the HSS, is presented in Fig. 11. To compare the energy dissipation of each specimen, the calculated energy dissipated in any cycle (E_i) was normalized against the energy dissipation of a rigid – perfectly plastic, nonbuckling element with the same yield load as that of the specimen it is compared with. The energy dissipated by the rigid plastic element (RP_i) represents the hypothetical maximum value of energy dissipation for the test specimen subject to the same axial displacements. Normalizing the energy dissipated eliminates the effect of varying yield loads and displacements. In return, the comparison of specimens with various loading histories and yield loads is facilitated. The value given by E_i/RP_i represents the energy dissipation efficiency of the test specimen. Specimens with smaller effective slenderness ratios show greater energy dissipation efficiency than those with larger effective slenderness ratios. This trend is observed in all specimens except specimen 2B. This specimen displayed more elastic behaviour prior to

Fig. 11. Cumulative specimen energy dissipation.

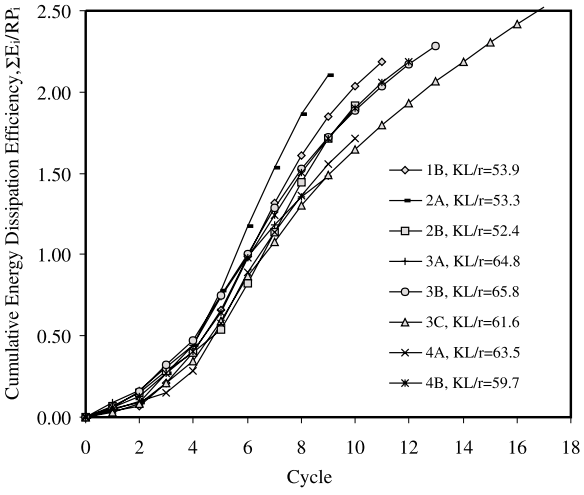

Fig. 12. Cumulative gusset energy dissipation.

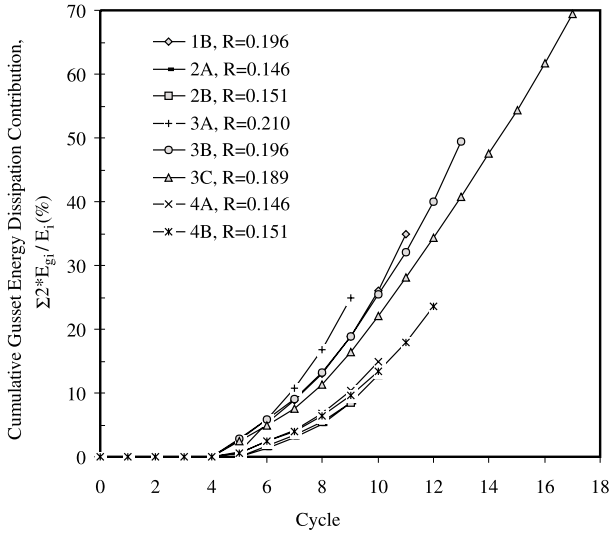

buckling and therefore dissipated less energy in the early cycles of testing.

The energy dissipated by the end connections was determined using the flexural stiffness of the gusset plate and its plastic rotation based on a simplified displacement model of the complete brace. The area enclosed in the moment-rotation curve for the gusset plate is equal to the energy dissipated by the gusset. Although the connections do not dissipate a significant amount of energy when compared with that of the HSS, it is useful to quantify this relationship to assist in developing end connections capable of dissipating greater amounts of energy while maintaining stable behaviour under large rotations due to brace buckling.

The cumulative energy dissipated by the gussets as a percentage of the energy dissipated by the specimen as a whole for each cycle of loading is shown in Fig. 12. A general pattern emerges from the figure, whereby the specimens with a greater strength ratio (R) show a slight increase in energy dissipation with respect to the total specimen for a given loading cycle. R is defined as the ratio of the plastic moment of the gusset plate to the plastic moment of the HSS section. The relationship between the gusset contributions in response to a change in the strength ratio is clearly shown in Fig. 12. All specimen end connections behaved very well; stable plastic behaviour was evident under the large lateral displacements experienced.

Conclusions

Two equations (eqs. [3] and [4]) were developed to predict the out-of-plane deflection of a buckling brace. Equation [3], based on a geometrical model of a buckled brace, can be used as an approximate prediction for the deflection. Equation [4], developed from and calibrated against the data from this series of tests, provides a more accurate prediction of the out-of-plane deflection.

The reduced compressive capacity lower bound, C_r', of a buckled brace appears to be nonconservative when compared with the results derived from this series of tests. This is due in part to the particular loading sequence employed. Nevertheless, this finding, also identified by Archambault (1995), suggests that the standard equation needs to be used with caution and that actual loading histories may result in lower residual compressive capacities.

The experimental fracture life of an HSS section brace is most affected by the width to thickness ratio of the HSS walls. The effective slenderness ratio and yield strength have a less significant effect on the fracture life. Maintaining many of the relationships in the fracture life prediction of Archambault (1995) and adding the data from this series of tests, a new equation, eq. [9], was developed to predict the theoretical fracture life of HSS sections that develop local buckling and subsequent material fracture.

The effective slenderness ratio, KL/r, is the single most important parameter influencing the hysteretic behaviour of the specimens tested. Although the wall width to thickness ratio of the brace influences the brace fracture life, it has a minimal effect on the hysteretic behaviour.

The energy dissipated by the gusset plate end connections accounted for less than 10% of the total energy dissipated by the specimens for a given cycle of loading. On average, the energy dissipated by the gussets was less than 4% of the total energy dissipated. The energy dissipation contribution of the gusset plates increased as the strength ratio between the HSS and gusset increased.

Acknowledgements

The writers wish to thank the following local companies for their support: TSE Steel Ltd., and Canam Steel Works. Omega Joists Inc., Triangle Steel, Three Star Steel, Moli Industries, Atlas Steel, R.I.M.K. Industries, Academy Steel, Renbec Industries, Infasco, Sureway Metal Systems, Airpac, and Reliable Tube provided further assistance. Without the aforementioned support this research would not have been possible. The work was also supported by the Natural Sciences and Engineering Research Council of Canada through an operating grant to the second author (RGP 203059-98) and the Steel Structures Education Foundation through a Research Grant Award. The expertise and assistance of the technical staff of the M.A. Ward Civil Engineering Labora-

tories at the University of Calgary have also been greatly appreciated.

References

AISC. 1999. Load and resistance factor design specification for structural steel buildings. American Institute of Steel Construction (AISC), Chicago, Ill.

Archambault, M.-H. 1995. Étude du comportement séismique des contreventements ductiles en X avec profiles tubulaires en acier. Report EPM/GCS-1995-09, Department of Civil Engineering, École Polytechnique, Montréal, Que.

Astaneh-Asl, A., Goel, S.C., and Hanson, R.D. 1985. Cyclic out-of-plane buckling of double angle bracing. ASCE Journal of Structural Engineering, **111**(5): 1135–1153.

Bruneau, M., Uang, C., and Whittaker, A. 1998. Ductile design of steel structures. McGraw-Hill, New York.

Cheng, J.J.R., Kulak, G.L., and Khoo, H. 1998. Strength of slotted tubular tension members. Canadian Journal of Civil Engineering, **25**(6): 982–991.

CSA. 1994. Limit states design of steel structures. Standard CAN/CSA-S16.1-94, Canadian Standards Association, Toronto, Ont.

CSA. 2001. Limit states design of steel structures. Standard CAN/CSA-S16-01, Canadian Standards Association, Toronto, Ont.

Galambos, T.V. (*Editor*). 1998. Guide to stability design criteria for metal structures. Technical Memorandum No. 3. 5th ed. John Wiley and Sons Inc., New York. pp. 814–822.

Hassan, O.F., and Goel, S.C. 1991. Modeling of bracing members and seismic behaviour of concentrically braced steel structures. Report UMCE 91-1, Department of Civil Engineering, The University of Michigan, Ann Arbor, Mich.

Jain, A.K., Goel, S.C., and Hanson, R.D. 1978. Inelastic response of restrained steel tubes. ASCE Journal of the Structural Division, **104**(6): 897–910.

Kahn, L.F., and Hanson, R.D. 1976. Inelastic cycles of axially loaded steel members. ASCE Journal of the Structural Division, **102**(ST5): 947–959.

Korol, R.M. 1996. Shear lag in slotted HSS tension members. Canadian Journal of Civil Engineering, **23**(6): 1350–1354.

Lee, S., and Goel, S.C. 1987. Seismic behavior of hollow and concrete-filled square tubular bracing members. Report UMCE 87-11, Department of Civil Engineering, The University of Michigan, Ann Arbor, Mich.

Popov, E.P., and Black, R.G. 1981. Steel struts under severe cyclic loadings. ASCE Journal of the Structural Division, **107**(ST9): 1857–1881.

Tang, X., and Goel, S.C. 1987. Seismic analysis and design considerations of braced steel structures. Report UMCE 87-4, Department of Civil Engineering, University of Michigan, Ann Arbor, Mich.

Tremblay, R., Bruneau, M., Nakashima, M., Prion, H.G.L., Filiatrault, A., and DeVall, R. 1996. Seismic design of steel buildings: lessons from the 1995 Hyogo-ken Nanbu earthquake. Canadian Journal of Civil Engineering, **23**(3): 727–756.

List of symbols

A	gross cross-sectional area of HSS
b	clear distance between webs, less the inside corner radius on each side
b/t	width to thickness ratio of compression element
C_r	compressive resistance of an axially loaded member
C_r'	reduced compressive resistance of an axially loaded member
C_s	experimentally determined fracture life constant
d	outside depth of HSS
E	Young's modulus of elasticity
E_{gi}	energy dissipation by gusset plate in cycle i
E_i	energy dissipation by full specimen in cycle i
E_i/RP_i	energy dissipation efficiency of specimen
F_y	specified yield strength
K	effective length factor
KL/r	effective slenderness ratio
L	overall specimen length
L/r	slenderness ratio
n	parameter for compressive resistance
P	axial load
$P_{\mathrm{comp\ max}}$	maximum compressive axial load in a cycle
P_y	axial yield load of a member
r	radius of gyration
R	strength ratio
RP_i	energy dissipation by a rigid, plastic nonbuckling element
t	thickness of flange or tube wall
Δ	lateral deflection of brace midspan
Δ/L	normalized out of plane deflection
Δ_1	normalized deformation from $P_y/3$ to the point of maximum compressive deformation
Δ_2	normalized deformation from the point at $P_y/3$ to the point of maximum tensile deformation
Δ_f	theoretical fracture life prediction
$\Delta_{f\ exp}$	experimentally determined fracture life of brace
δ	axial displacement of brace end
δ_y	axial yield deflection
λ	nondimensional slenderness parameter in column formula
μ	ductility ratio or flexural stiffness coefficient of connection